Estimating the Hubble Constant via Gravitational Waves

Author: 219046104[1]
Supervisor: Prof. Nial Tanvir[2,]

Department of Physics and Astronomy, University of Leicester

April 29, 2025

ABSTRACT

Context. The precise measurement of the Hubble constant (H_0), which governs the expansion rate of the Universe, remains a major challenge in cosmology. Discrepancies between early- and late-Universe measurements, known as the "Hubble tension," have motivated alternative approaches independent of the traditional cosmic distance ladder. Gravitational-wave dark standard sirens—binary black hole (BBH) mergers without electromagnetic counterparts—offer a promising, complementary method for estimating H_0 using statistical host galaxy association.
Aims. This study aims to simulate the inference of H_0 using a population of mock BBH mergers and a realistic galaxy catalogue. We seek to validate a likelihood-based host association framework, recover frequentist point estimates of H_0, and quantify statistical uncertainties through Monte Carlo resampling and Bayesian analysis.
Methods. Gravitational-wave distance measurements were simulated with 30% Gaussian uncertainty, and sky localizations were modelled using a truncated von Mises–Fisher distribution with a 5° angular spread. Candidate host galaxies were selected from EAGLE simulation data, filtered by stellar mass. For each merger event, joint angular and distance likelihoods were computed over all galaxies. Summing and maximizing these likelihoods across events provided frequentist estimates of H_0, while resampling generated uncertainty bounds. A Bayesian posterior distribution for H_0 was also constructed by multiplying likelihoods across independent events.
Results. Across four independent realizations with $N_{\mathrm{merger}} = 100$ events each, recovered Hubble constants clustered between 68.0 and 72.0 $\mathrm{km\,s^{-1}\,Mpc^{-1}}$, consistent with the true input value (67.0 $\mathrm{km\,s^{-1}\,Mpc^{-1}}$) within uncertainties. The Bayesian posterior yielded $H_0 = 72.0^{+17.9}_{-19.8}$ $\mathrm{km\,s^{-1}\,Mpc^{-1}}$, with the 68% credible interval covering approximately 60% of the uniform prior range [40, 100] $\mathrm{km\,s^{-1}\,Mpc^{-1}}$. Monte Carlo noise was mitigated via spline fitting of likelihood curves.
Conclusions. Our results demonstrate that gravitational-wave dark sirens, even in the absence of electromagnetic counterparts, can provide meaningful constraints on H_0. Combining frequentist point estimation, Bayesian posterior construction, and Monte Carlo uncertainty quantification yields a robust framework. Scaling to larger event samples and improved galaxy catalogues will be critical to achieving competitive precision and addressing the Hubble tension in the coming era of gravitational-wave cosmology.

Key words.

1. Introduction

Determining the Hubble constant—the rate at which the universe expands—remains one of the most compelling challenges in modern cosmology. Traditionally, estimates have hinged on electromagnetic observations, such as those from Type Ia supernovae. However, the advent of gravitational wave astronomy has introduced an independent, promising alternative: standard sirens. These gravitational wave signals, emerging from the mergers of compact objects like neutron stars and binary black holes, offer a novel way to measure cosmic distances without the intermediary steps required by traditional methods.

The increasing sensitivity and frequency of gravitational wave detections have propelled standard sirens into the spotlight. Yet, the task of precisely estimating the Hubble constant through these means is fraught with challenges—from inherent measurement uncertainties to the complexities of modelling astrophysical sources. In response to these challenges, this report presents a new simulation-based method designed to refine the estimation process using standard siren data.

The simulation framework developed herein seeks to realistically replicate both the generation and detection of gravitational wave signals. By incorporating detailed noise models and astrophysical parameters, the method allows for a comprehensive examination of how various factors impact the derived value of the Hubble constant.

1.1. Cosmic Expansion

The fundamental understanding of modern-day cosmology is the discovery that our universe is not static but is in a state of expansion and understanding how fast the universe is expanding, leading to determination of the age of the universe. It would be easy to start by conceptualising this idea by visualising the common balloon analogy. Imagine drawing dots on the surface of a deflated balloon, each dot representing a galaxy. As the balloon inflates, the distance between any two dots increases even though the dots themselves are not "moving" across the balloon's surface in

the usual sense; instead, the surface (analogous to space) is stretching.

1.2. Hubble Law and its Discovery

In 1929, Edwin Hubble published his seminal paper, which showed a relationship between the distance to "extra-galactic nebulae" (what we now call galaxies) and their recessional velocities, measured via redshifts. This discovery built on earlier measurements of spectral shifts by Vesto Slipher, who first noted that many spiral nebulae were redshifted, suggesting they were receding from us.

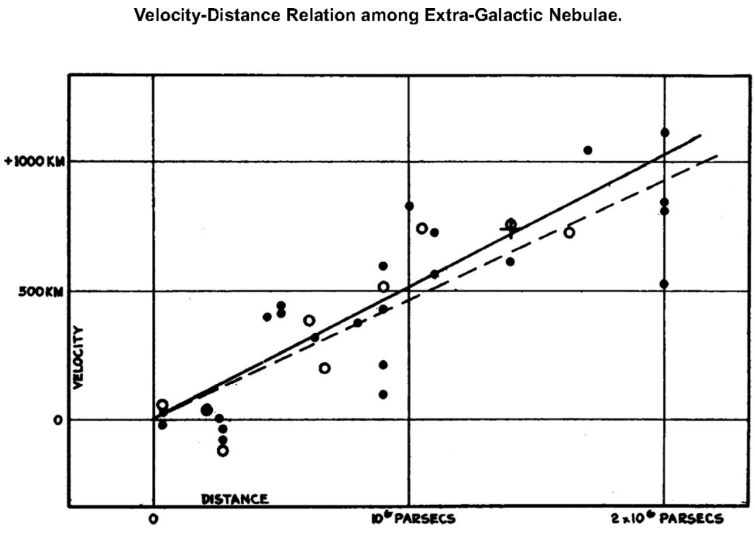

Fig. 1: Radial velocities, adjusted for solar motion, are plotted against distances estimated from the stars involved and the average luminosity of nebulae within a cluster (Hubble 1929). The black discs with the solid line show the solar motion solution when using each nebula individually; the circles with the dashed line show the solution when the nebulae are grouped together; and the cross indicates the average velocity for 22 nebulae whose individual distances could not be determined (Hubble 1929). (Note: Velocity is measured in kilometers per second.)

Hubble used Doppler shifts of spectral lines to determine how fast a galaxy is moving away from us. When light from a distant galaxy shifts toward the red end of the spectrum, it indicates that the source is receding. Determining the distance to galaxies was (and still is) a challenging task. In Hubble's time, he relied on Cepheid variable stars to gauge distances to nearby galaxies; these stars have a well-known period–luminosity relationship, allowing astronomers to estimate how far away they are. Over time, astronomers developed a "distance ladder," which extends to more distant galaxies using supernovae or other standardized candles.

Hubble plotted the recessional velocity of galaxies against their distance and found an approximately linear trend. This direct proportionality between velocity and distance is now called Hubble's Law:

$$v = H_0 d \quad (1)$$

where v is the galaxy's recession velocity, d is its distance, and H_0 (the Hubble constant) is the slope of the line i.e. the current expansion rate of the universe.

1.3. Observational Techniques and Measurement Methods

One of the primary methods for measuring H_0 is the local distance ladder, which utilizes the distances to nearby galaxies. This technique often involves calibrating the luminosity of Cepheid variable stars, which act as standard candles. Through extensive measurements, the SH0ES (Supernovae and H_0 for the equation of state) collaboration determined H_0 to be approximately 73.24 ± 1.74 kms^{-1} Mpc^{-1} based on Cepheid distances and Type Ia supernovae observations (Riess et al. 2016; Lu and Gong 2023). This method capitalizes on accurate parallax measurements and local stars, providing significant precision, but it is dependent on the assumption that extinction effects and distances are well understood. Recent recalibrations of the distance ladder have refined these measurements further, demonstrating progress from systematic errors (Lu and Gong 2023).

Another pivotal approach is the analysis of the Cosmic Microwave Background (CMB) radiation. Measurements from the Planck satellite have provided an H_0 value around 67.4 ± 0.5 km s^{-1} Mpc^{-1}, derived from the physics of the early universe, specifically analyzing anisotropies in the CMB (Zhou 2023; Pesce et al. 2020). This method operates within the framework of the Lambda Cold Dark Matter (ΛCDM) model and relies on understanding the cosmic composition and dynamics at high redshifts.

Gravitational wave standard sirens represent yet another innovative methodology for H_0 measurement, which utilizes the observed waveforms from merging black holes and neutron stars. For instance, the LIGO/Virgo collaborations employed the distance measured from the gravitational waves emitted during events like GW170817, along with electromagnetic observations, to derive an H_0 value of around 70 km s^{-1} Mpc^{-1} (Abbot et al. 2017; Chen et al. 2018). This method circumvents many of the conventional distance ladder dependencies, fostering a new avenue for determining cosmological parameters reliably.

In conclusion, the determination of the Hubble constant is a multifaceted endeavor that requires diverse methodologies to triangulate a reliable estimate. Each method—local distance ladders, CMB measurements, and gravitational wave standard sirens contributes distinct insights but also reflects the complexities and systemic errors intrinsic to cosmological measurements. The ongoing dialogue within the astrophysics community seeks to mitigate these tensions, aiming to refine the standard cosmological model and enhance our grasp of universal expansion.

1.4. Hubble Tension

The Hubble tension refers to the significant discrepancy observed between measurements of the Hubble constant, (H_0), derived from different cosmological approaches. Specifically, local measurements using Type Ia supernovae calibrated through Cepheid variable stars by the SH0ES team yield a Hubble constant around (73.8 ± 2.4 , km s^{-1} Mpc^{-1}) (Friedman 2025; Lopez-Hernandez and De-Santiago 2025; Mostaghel 2022). In contrast, measurements derived from cosmic microwave background (CMB)

observations, particularly by the Planck satellite under the standard Lambda Cold Dark Matter (ΛCDM) model, suggest a lower value, approximately (67.4 ± 0.6 , km s^{-1} Mpc^{-1}) (Tiwari et al. 2023; Costa et al. 2024; Verde et al. 2019). This inconsistency, reaching over 4σ in statistical significance, has generated substantial debate within the cosmological community regarding the implications for our understanding of the universe's expansion dynamics and the underlying physics driving it (Hsiao et al. 2022).

The importance of resolving the Hubble tension lies not only in refining the precise value of (H_0) but also in testing and potentially extending our current cosmological models. Various alternative theories and models have been proposed to explain this discrepancy, including modifications to dark energy models, such as introducing late-time dynamics that could adjust the expansion rate of the universe (Friedman 2025; Neukart 2024). Additionally, self-interacting neutrinos have been suggested as another mechanism that could account for differences in measurements; however, such models face strict constraints from other observational data (Das and Ghosh 2022).

Moreover, the implications of the Hubble tension extend beyond simple measurement discrepancies; they challenge fundamental cosmological principles. For instance, the necessity to modify or extend the ΛCDM model raises questions about the nature of dark matter and dark energy. Some researchers argue that the tension might hint at a deeper unification of these components of the universe's structure (Burenin 2013; Gurzadyan 2019). Furthermore, systematic errors in measurement techniques, especially concerning calibration of standard candles in different redshift regimes, contribute to ongoing scrutiny and debate (Wang and Meng 2014; Bolejko 2018).

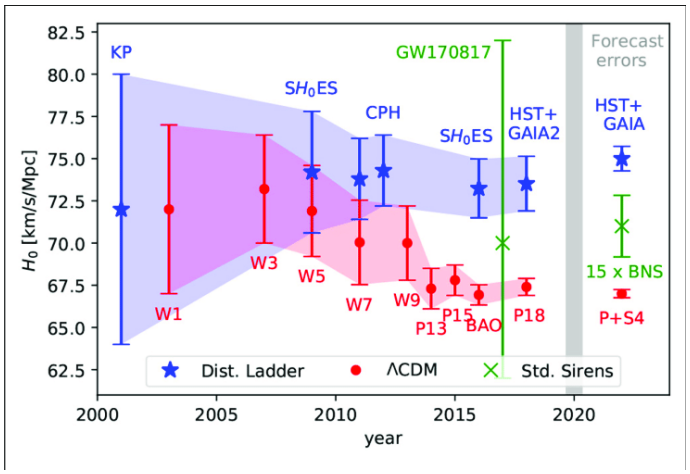

Fig. 2: The first standard siren measurement after the GW170817 event (Abbott et al. 2017*a*), data from Planck 2018 (Aghanim et al. 2020), and Hubble Space Telescope (HST) observations in conjunction with GAIA DR2 (Riess et al. 2018) are all included in the Hubble tension as depicted (Beaton et al. 2016).

1.5. Gravitational Wave Detection for Standard Sirens

Gravitational waves are produced when two compact objects, like black holes or neutron stars, merge and spiral inward. Observations like Virgo and LIGO can detect these waves. A merger of a binary black hole (BBH) is considered "dark" since it only produces gravitational waves and no electromagnetic (EM) radiation. On the other hand, they are especially useful for "standard siren" analyses that improve localization and allow the determination of cosmological parameters because binary neutron star (BNS) mergers produce both gravitational waves and their electromagnetic counterparts, such as gamma-ray bursts (Abbott et al. 2017*b*). Laser interferometry, which LIGO and Virgo use, is the main method for detecting gravitational waves. These detectors use the interference patterns of laser beams moving along the arms as a gravitational wave passes through to measure extremely small changes in the lengths of L-shaped vacuum tubes—on the order of 10^{-18} meters (LIGO Lab 2024).

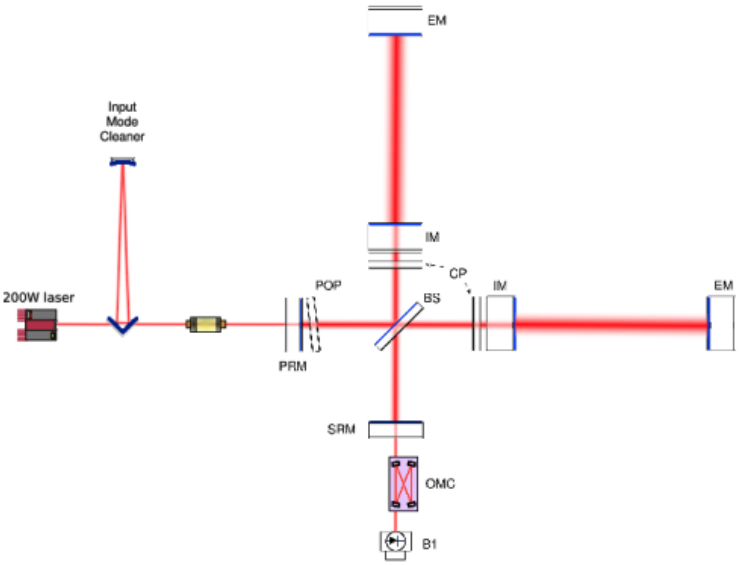

Fig. 3: A simplified optical configuration of Advanced VIRGO is based on the Michelson interferometer architecture. In this design, each arm contains a Fabry-Perot resonant optical cavity, created by the arrangement of an Input Mirror (IM) and an End Mirror (EM), which serves to effectively increase the optical path length and enhance the sensitivity to passing gravitational waves. To further boost the detector's performance, a Power Recycling Mirror (PRM) is placed at the laser input to increase the circulating power within the interferometer, and a Signal Recycling Mirror (SRM) is installed at the output port to optimize the frequency response and bandwidth of the detector. This advanced configuration enables VIRGO to detect extraordinarily small spacetime distortions caused by gravitational wave events with greater precision and across a broader frequency range (Cella 2017)

Modern interferometers such as Virgo and LIGO have transformed our capacity to quantify the minuscule spacetime distortions brought about by gravitational waves. In order to detect changes in path length, their basic design

is based on a Michelson interferometer, which divides a laser beam into two perpendicular arms that reflect off mirrors and recombine. A simplified optical layout of the Advanced VIRGO detector is shown in Figure 3. A Fabry-Perot resonant cavity is incorporated into each arm between an input mirror (IM) and an end mirror (EM), effectively lengthening the optical path and improving sensitivity. Moreover, the inclusion of Power Recycling (PRM) and Signal Recycling (SRM) mirrors increases the circulating laser power and enhances the bandwidth of the detector (Cella 2017). This arrangement enables interferometers such as VIRGO and LIGO to identify displacements as tiny as 10^{-18} meters, which is equivalent to a change that is less than a nanometer in diameter.

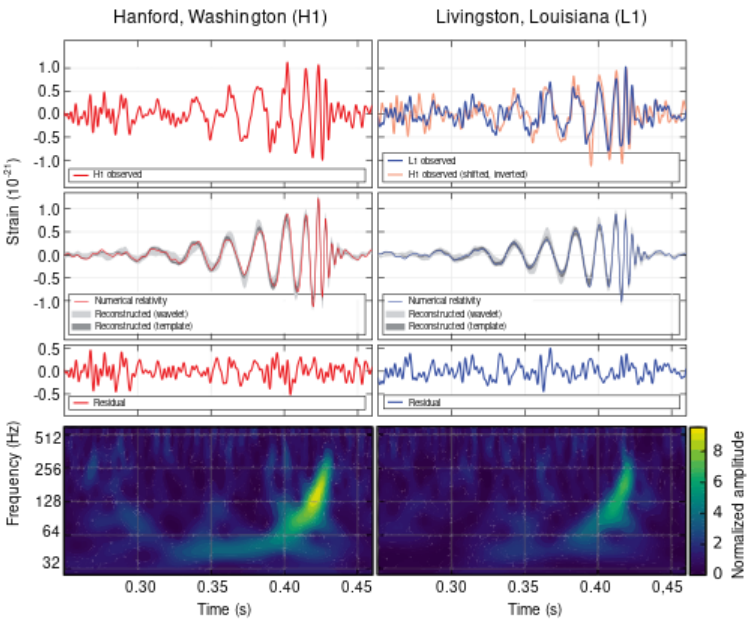

Fig. 4: The plots illustrate the first direct detection of gravitational waves. The top left panel shows the filtered signal from LIGO Hanford (H1), while the top right panel overlays the time-shifted and sign-corrected signal from LIGO Livingston (L1) with H1. The bottom panels present a comparison between the measured signals and numerical relativity models, demonstrating strong agreement. Adapted from (Abbott et al. 2016)

.

The first direct detection of gravitational waves was made possible by the LIGO Scientific Collaboration in 2016 thanks to the instruments' unparalleled sensitivity. Figure 4 displays the main findings from this landmark observation. Hanford (H1) and Livingston (L1), LIGO's two detectors, provide the filtered gravitational-wave signals displayed in the top panels. The signals from the two detectors align exceptionally well after a 7 millisecond time correction and sign inversion. The bottom panels confirm the merger of two stellar-mass black holes by comparing the observed signals with numerical relativity models, showing excellent agreement (Abbott et al. 2016). By confirming the identification and theoretical modelling of gravitational wave sources, this agreement establishes gravitational wave astronomy as a novel and autonomous universe probe.

2. Standard Sirens

Standard sirens are astrophysical sources whose luminosity distance can be measured independently of traditional cosmic distance ladders, making them valuable tools for cosmological studies. They typically arise from gravitational wave (GW) events, particularly mergers of compact binaries such as binary neutron stars (BNS) and binary black holes (BBH). When GWs are emitted from these events, the intrinsic properties of the signal allow for a direct measurement of luminosity distance based solely on the amplitude of the gravitational waves received on Earth, which is analogous to how standard candles (like Type Ia supernovae) operate in the realm of electromagnetic observations.

2.1. Bright Sirens

Bright sirens are a particular class of gravitational wave (GW) sources that provide a unique method for measuring cosmological parameters, specifically the Hubble constant (H_0) (Schutz 1986; Holz and Hughes 2005). This category of "standard sirens" is characterized by the presence of accompanying electromagnetic (EM) counterparts which are crucial for identifying the source's redshift, thereby allowing for a more accurate construction of distance–redshift relations (Nissanke et al. 2010). This property distinguishes bright sirens from their counterparts known as dark sirens, which lack such EM observations and rely on galaxy catalogues to estimate redshifts (Gray et al. 2020).

The primary sources of bright sirens are typically binary neutron star (BNS) mergers. These events often yield significant EM signals such as kilonovae or short gamma-ray bursts (GRBs) that can be observed concurrently with the gravitational waves they emit (Metzger and Berger 2012). The landmark event GW170817 marked the first detection that firmly established the application of bright sirens in cosmology, as it was linked to notable electromagnetic emissions that allowed scientists to pinpoint the event's distance and redshift (Abbott et al. 2017*b*). Because these measurements do not depend on calibrating supernovae or other traditional methods, bright sirens provide an independent avenue for measuring H_0 and exploring cosmic expansion.

The methodology of using bright sirens for measuring the Hubble constant involves two main components: the gravitational wave signal itself, which provides the luminosity distance, and the redshift derived from the EM counterpart (Chen et al. 2018). By plotting these two quantities together, researchers can create a Hubble diagram that facilitates cosmological analysis. Forecasts indicate that with next-generation gravitational wave observatories and sufficient event rates, bright sirens could constrain H_0 to subpercent precision over several years of data collection (Chen et al. 2018; Borhanian and Sathyaprakash 2022).

2.2. Dark Sirens

Dark sirens refer to gravitational-wave (GW) sources that lack electromagnetic (EM) counterparts, necessitating statistical methods to infer their cosmological parameters, particularly the redshift (Del Pozzo 2012; Gray et al. 2020).

This approach is crucial in gravitational-wave cosmology as it allows one to derive important measurements of the Hubble constant H_0 from events without directly observable EM signals, such as gamma-ray bursts or optical counterparts (Fishbach et al. 2019). Since EM observations are absent, astronomers cannot assign a redshift—i.e. the amount by which wavelengths have been stretched by cosmic expansion—directly from data. Instead, they exploit the intrinsic relation between GW amplitude and luminosity distance d_L, which follows from the signal's frequency and amplitude evolution (Schutz 1986; Holz and Hughes 2005).

To recover redshift from dark sirens, detected GW events are statistically cross-correlated with galaxy catalogues (Soares-Santos 2019). Each event's sky-localization volume defines the three-dimensional region where its host galaxy might reside (Gray et al. 2020). Within that volume, candidate galaxies are weighted by properties such as stellar mass or star-formation rate (Smith and Johnson 2021), yielding a probability distribution over possible redshifts. Summing these probabilities over all galaxies produces a posterior $p(z \mid \mathrm{GW})$, which can then be converted via $d_L(z; H_0)$ into a posterior on H_0. By marginalizing over the entire galaxy set, the dark-sirens method delivers a fully statistical estimate of H_0 in the absence of any direct EM counterpart.

3. Modelling Dark Sirens Environment

To generate a realistic set of binary black hole (BBH) merger sites within our $(0\text{–}100\,\mathrm{Mpc})^3$ simulation volume, we begin by treating each galaxy in the catalogue as a potential host. From its Cartesian coordinates (x_i, y_i, z_i) we compute the true luminosity distance $d_{\mathrm{true},i}$. We then assign to each galaxy a mock gravitational-wave distance $d_{\mathrm{GW},i}$ by drawing from a Gaussian distribution centred on $d_{\mathrm{true},i}$ with fractional width α.

Next, to emulate the uncertainty in sky localization inherent to gravitational-wave detectors, we sample an angular displacement around each galaxy's line of sight from a Fisher distribution (the von Mises–Fisher equivalent on the sphere). Specifically, for each event we draw a unit vector $\hat{n}$ with concentration parameter κ, so that the probability density of observing an offset angle θ from the true direction is

$$p(\hat{n}|\boldsymbol{\mu}, \kappa) \propto \exp\big(\kappa\, \boldsymbol{\mu} \cdot \hat{n}\big)\,, \tag{2}$$

where $\boldsymbol{\mu}$ points toward the galaxy. Multiplying $\hat{n}$ by $d_{\mathrm{GW},i}$ yields the perturbed merger location (x_i', y_i', z_i').

By repeating this procedure for all galaxies, our simulation produces a three-dimensional catalogue of BBH merger positions that incorporate both distance uncertainty and realistic angular localization error.

3.1. 3D Galaxy Distribution

The EAGLE simulation - short for Evolution and Assembly of GaLaxies and their Environment is a large-scale cosmological hydrodynamical simulation designed to study the formation and evolution of galaxies over cosmic time (Schaye et al. 2015; Crain et al. 2015). Using the data provided by the EAGLE simulation, an artificial density space consisting of galaxy cluster, each a potential host for a binary black hole merger in a 100 Mpc^3 Mpc volume of sky is sampled uniformly to create a robust cosmic distribution for the simulation and the estimation of the Hubble constant.

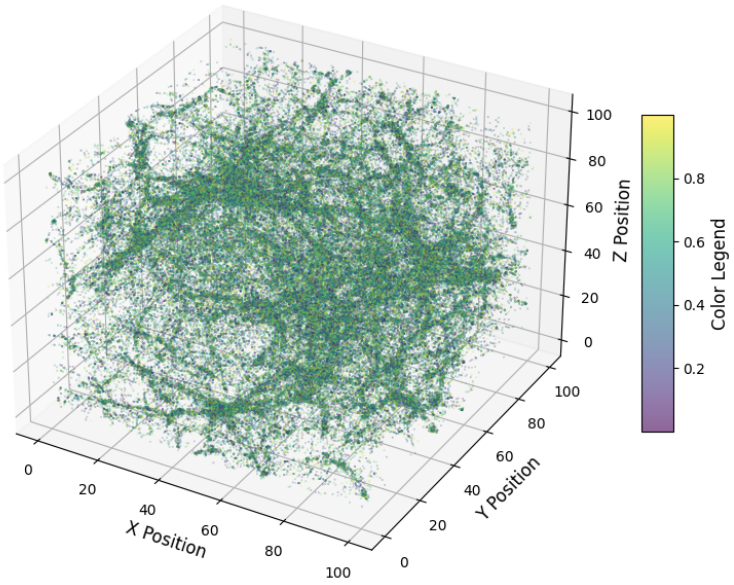

Fig. 5: Three-dimensional distribution of simulated galaxies within a $(0\text{–}100\,\mathrm{Mpc})^3$ co-moving volume. Each point marks a galaxy's Cartesian position (x, y, z) in Mpc, and the color scale serves to distinguish individual objects and enhance depth perception. The filamentary network of the cosmic web—dense knots connected by filaments and interspersed with voids—is clearly visible.

3.2. Simulation of Gravitational-Wave Distances

Each galaxy in our sample is treated as a potential gravitational-wave host. We compute its true luminosity distance from the origin,

$$d_{\mathrm{true}} = \sqrt{x^2 + y^2 + z^2}\,,$$

using its Cartesian coordinates (x, y, z). To model the uncertainty in a gravitational-wave–inferred distance d_{GW}, we assume

$$d_{\mathrm{GW}} \sim \mathcal{N}\big(d_{\mathrm{true}},\, (\alpha\, d_{\mathrm{true}})^2\big),$$

with an initial fractional error $\alpha = 0.3$ (i.e. a 30% 1σ uncertainty). For each galaxy we draw N realizations of d_{GW} and form the ratio

$$r = \frac{d_{\mathrm{GW}}}{d_{\mathrm{true}}}\,.$$

Figure 6 shows the histogram of these ratios for a representative galaxy. The dashed red curve is a Gaussian fit,

$$n(r) = A \exp\Big[-\tfrac{(r-\mu)^2}{2\,\sigma_{\mathrm{fit}}^2}\Big],$$

which returns $\sigma_{\mathrm{fit}} \approx 0.30$, in close agreement with our input α. The vertical blue line at $r = 1$ indicates perfect recovery of the true distance.

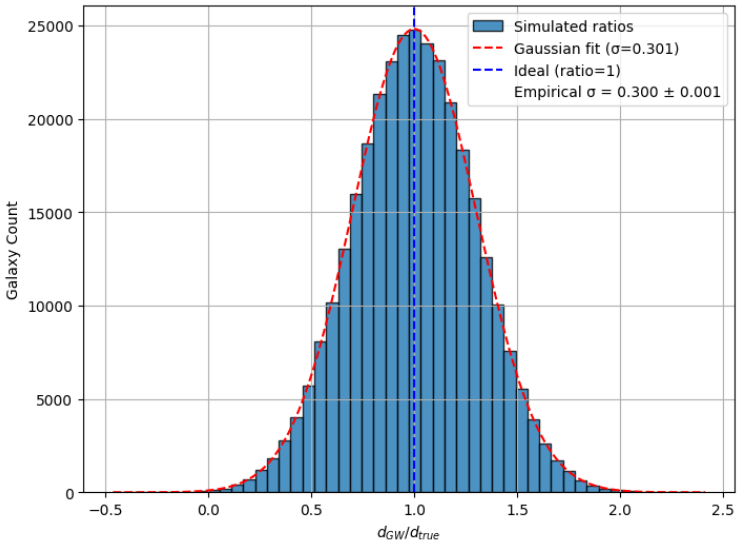

Fig. 6: Histogram of the ratio $d_{\rm GW}/d_{\rm true}$ for a representative galaxy. The dashed red curve is the best-fit Gaussian.

3.3. Directional Perturbation of Host Galaxies

Gravitational wave interferometers typically localize compact-binary coalescences to extended sky regions rather than pinpoint coordinates. The resulting angular uncertainty, which can range from a few degrees to tens of degrees depending on network configuration and signal-to-noise ratio, must be propagated into any three-dimensional merger catalogue. Moreover, to reflect the fact that binary black hole mergers preferentially occur in sufficiently massive hosts, we impose a stellar-mass threshold: only galaxies with $M_\star \geq 10^6\,M_\odot$ are considered as potential hosts. This cut ensures that each selected galaxy harbors a large enough stellar population to produce the progenitor binaries and to be detectable in current surveys. We therefore perturb each galaxy's true line of sight by random polar and azimuthal offsets in order to emulate the detector localization error.

A host galaxy is first selected at random within the cubic volume $(100\,\mathrm{Mpc})^3$. Denoting its Cartesian coordinates by (x_0, y_0, z_0), one defines the position vector and its normalization as

$$\mathbf{g} = (x_0,\, y_0,\, z_0), \qquad \|\mathbf{g}\| = \sqrt{x_0^2 + y_0^2 + z_0^2},$$

and the corresponding unit sightline

$$\hat{\mathbf{g}} = \frac{\mathbf{g}}{\|\mathbf{g}\|}\,.$$

An angular deviation θ from the true direction is drawn from a prescribed error distribution—commonly a von Mises–Fisher distribution with concentration κ. To parameterize directions at angle θ from $\hat{\mathbf{g}}$, an orthonormal basis $\{\mathbf{u}_1, \mathbf{u}_2\}$ spanning the plane perpendicular to $\hat{\mathbf{g}}$ is constructed by selecting a reference axis $\hat{\mathbf{e}}_x$ and computing

$$\mathbf{u}_1 = \frac{\hat{\mathbf{g}} \times \hat{\mathbf{e}}_x}{\|\hat{\mathbf{g}} \times \hat{\mathbf{e}}_x\|}, \qquad \mathbf{u}_2 = \hat{\mathbf{g}} \times \mathbf{u}_1,$$

ensuring $\hat{\mathbf{g}} \perp \mathbf{u}_1, \mathbf{u}_2$ and $\mathbf{u}_1 \perp \mathbf{u}_2$.

An azimuthal angle ϕ is then sampled uniformly in $[0, 2\pi)$, and a unit offset in the tangent plane is defined by

$$\mathbf{r} = \sin\theta\,\big(\cos\phi\,\mathbf{u}_1 + \sin\phi\,\mathbf{u}_2\big).$$

By combining this tangential component with the polar projection, the perturbed unit direction

$$\hat{\mathbf{b}} = \cos\theta\,\hat{\mathbf{g}} + \mathbf{r}$$

is obtained, which remains normalized by construction. Finally, if $d_{\rm GW}$ denotes the luminosity distance inferred from the gravitational-wave measurement (with its own radial uncertainty model), the three-dimensional merger location is placed at

$$\mathbf{b} = d_{\rm GW}\,\hat{\mathbf{b}}.$$

This angular-offset sampling procedure thus "jitters" each galaxy's true sightline by an angle θ with random azimuth ϕ, embedding both the detector's localization error and the astrophysical host-mass selection into the simulated merger catalogue.

3.3.1. von-Mises Fisher Distribution

On the celestial sphere, each gravitational-wave source direction corresponds to a point on the unit two-sphere S^2, not to a point in an unbounded flat plane. A naive planar Gaussian in the polar angle θ and azimuth ϕ would ignore the fact that the available solid angle grows as $\sin\theta$. In particular, the surface element on the sphere is

$$\mathrm{d}\Omega = \sin\theta\,\mathrm{d}\theta\,\mathrm{d}\phi,$$

so any probability density $p(\theta, \phi)$ must integrate over S^2 with that Jacobian in order to normalize correctly. A simple Gaussian in θ,

$$p(\theta) = \frac{1}{\sqrt{2\pi\sigma^2}} e^{\frac{\theta}{2\sigma^2}},$$

would overweight mid-latitude angles relative to small deviations and fail to remain isotropic in ϕ.

By contrast, the von Mises–Fisher distribution on S^2,

$$p(\hat{\mathbf{x}}) \propto \exp\big(\kappa\,\hat{\mu}\cdot\hat{\mathbf{x}}\big),$$

naturally incorporates the $\sin\theta$ factor when expressed in (θ, ϕ) coordinates,

$$p(\theta) \propto \sin\theta\,\exp\big(\kappa\,\cos\theta\big),$$

and remains uniform in azimuth. Furthermore, it is the maximum-entropy distribution on the sphere for a given mean direction $\hat{\mu}$. In the small-angle limit $\theta \ll 1$, one recovers the familiar planar Gaussian form, since $\sin\theta \approx \theta$ and $\cos\theta \approx 1 - \theta^2/2$. However, for the multi-degree localization regions typical of current gravitational-wave detectors, faithfully modelling the curvature of S^2 is essential to avoid biasing the angular error distribution.

The angular localization error on the sky is naturally described by the von Mises–Fisher (vMF) distribution on the unit sphere. In terms of the polar angle θ (the separation between true and observed directions) and the azimuth ϕ, the joint density is

$$p(\theta, \phi)\,\mathrm{d}\Omega = \frac{\kappa}{2\pi\big(e^{\kappa} - e^{-\kappa}\big)}\, e^{\kappa\cos\theta}\,\mathrm{d}\Omega,$$

where κ is the concentration parameter and $\mathrm{d}\Omega = \sin\theta\,\mathrm{d}\theta\,\mathrm{d}\phi$ is the solid-angle element.

Marginalizing over ϕ gives the polar density

$$p(\theta) = \int_0^{2\pi} p(\theta,\phi)\,\mathrm{d}\phi = \frac{\kappa}{e^{\kappa} - e^{-\kappa}}\, e^{\kappa\cos\theta}\,\sin\theta\,, \qquad 0 \le \theta \le \pi$$

The cumulative distribution function for θ follows by direct integration:

$$F(\theta) = \int_0^{\theta} p(\theta')\,\mathrm{d}\theta' = \frac{e^{\kappa} - e^{\kappa\cos\theta}}{e^{\kappa} - e^{-\kappa}}\,.$$

In practice one draws a uniform random variate $u \in [0,1]$ and inverts $F(\theta) = u$ to obtain

$$\theta = \arccos\Big[\frac{1}{\kappa}\,\ln\big(e^{\kappa} - u\,(e^{\kappa} - e^{-\kappa})\big)\Big].$$

This procedure yields samples of the polar offset θ distributed according to the desired vMF kernel, automatically accounting for the $\sin\theta$ solid-angle measure and ensuring isotropy in the azimuth ϕ.

In our implementation, the von Mises–Fisher concentration parameter is tied directly to the total angular uncertainty,

$$\sigma_{\mathrm{tot}} = \sqrt{\sigma_{\mathrm{stat}}^2 + \sigma_{\mathrm{sys}}^2}, \qquad \kappa = \frac{1}{0.66\,\sigma_{\mathrm{tot}}^2},$$

where σ_{stat} and σ_{sys} are the statistical and systematic components of the localization error, respectively. Once κ is fixed, a large ensemble of polar offsets $\{\theta_j\}$ is generated by drawing uniform variates $u_j \in [0,1]$ and inverting the cumulative distribution

$$F(\theta) = \frac{e^{\kappa} - e^{\kappa\cos\theta}}{e^{\kappa} - e^{-\kappa}} \quad\Longrightarrow\quad \theta_j = F^{-1}(u_j). \tag{3}$$

To construct the angular distribution, the interval $[0,\theta_{\max}]$ is partitioned into N bins with edges $0 = \theta_0 < \theta_1 < \cdots < \theta_N = \theta_{\max}$. The theoretical probability in the ith bin is

$$P_i = F(\theta_i) - F(\theta_{i-1}),$$

while the simulated offsets are counted in the same bins to form an empirical histogram. Plotting P_i (or the normalized counts) against the bin centres θ_i produces a direct comparison of the expected vMF distribution to the Monte-Carlo sample.

Such a plot is important because it verifies that the chosen κ correctly encapsulates both statistical and systematic uncertainties, and it illustrates the fraction of events localized within small angular separations versus those in the tails. By comparing multiple realizations or varying σ_{tot}, one can assess how localization performance degrades with increasing error and quantify the probability of large mislocalizations in a statistically rigorous manner.

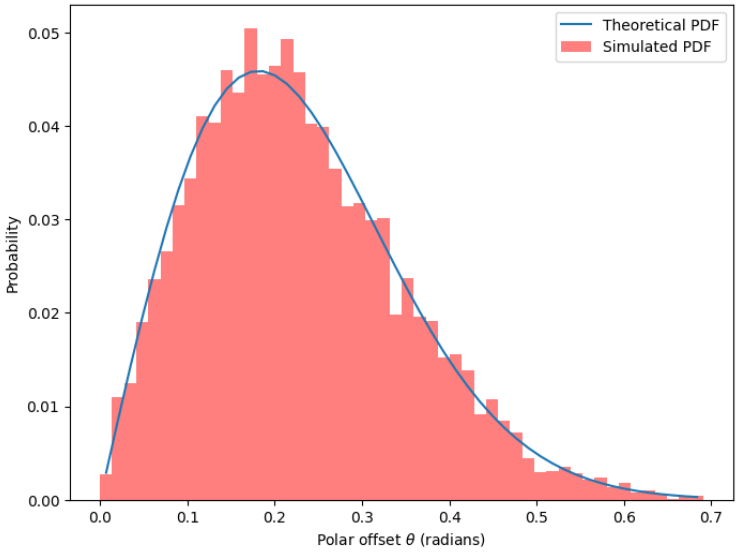

Fig. 7: Comparison between the simulated distribution of polar offsets θ (red histogram) and the theoretical truncated von Mises–Fisher probability density function (blue curve) used in the simulation. The close agreement between simulation and theory validates the implementation of the angular perturbation model used to mimic realistic gravitational-wave sky localizations.

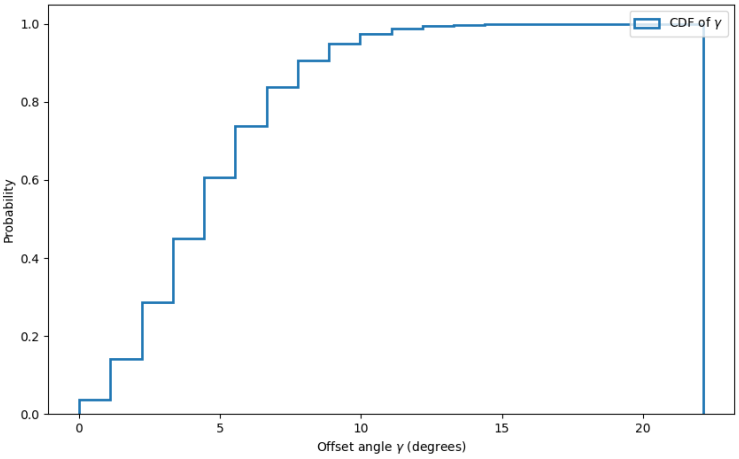

Fig. 8: Cumulative distribution function (CDF) of offset angles γ sampled from a truncated Fisher distribution around host galaxies' true positions. The x-axis shows the angular displacement in degrees, and the y-axis indicates cumulative probability. Approximately 50% of offsets lie within 5°–6°, and 90% within 12°, with all offsets truncated at 20°. This distribution models the angular uncertainty associated with gravitational-wave sky localizations, ensuring physically realistic perturbations of merger positions for dark standard siren analyses.

4. Recovering the Hubble Constant from Dark Standard Sirens

4.1. Inference Framework for H_0 Recovery

The dark standard siren approach leverages binary black hole (BBH) mergers as distance indicators without electromagnetic counterparts. Each event provides a well-

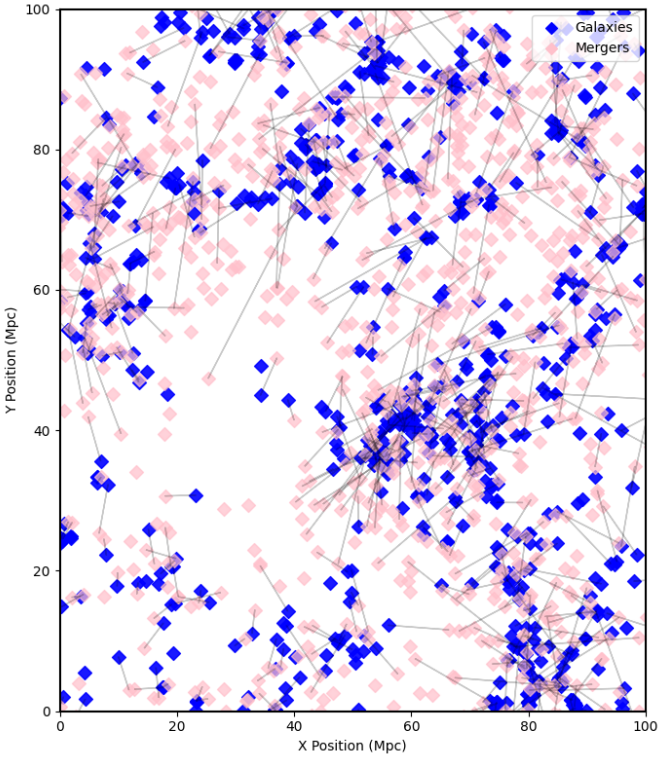

Fig. 9: Two-dimensional slice of the (100 Mpc)^3 simulation volume with 70 Mpc $\leq z \leq$ 100 Mpc, showing host galaxies (red dots) and their corresponding binary-black-hole merger locations (blue dots). Merger positions were generated by applying a von Mises–Fisher angular perturbation and a Gaussian radial uncertainty to each galaxy sight-line. Because only points within the chosen z-interval are plotted, the projected merger density appears enhanced and some host galaxies fall outside the sliced frame.

measured luminosity distance from its gravitational-wave signal but no direct redshift, so we associate it statistically with galaxies in a volume-limited catalog (filtered to stellar masses $M_\star \geq 10^6\, M_\odot$). To account for measurement uncertainty, every merger is "jittered" in angle—using a von Mises–Fisher distribution on the sphere—and in distance—using a Gaussian centered on the true luminosity distance.

These perturbed event positions are then compared against all candidate hosts: for each galaxy–event pair, the galaxy's comoving distance $d_{\rm true}$ predicts a recession velocity $v = H_0\, d_{\rm true}$ under any assumed Hubble constant. By evaluating how well the waveform-inferred distance matches v/H_0, and combining that radial likelihood with the angular probability of association, we build a joint likelihood for each event as a function of H_0. Multiplying (or summing log-likelihoods) over the full ensemble of mergers yields a total likelihood curve in H_0, whose maximum defines our recovered value $H_0^{\rm rec}$.

To estimate the statistical uncertainty of this recovery, we repeat the entire inference multiple times—each time drawing new angular and distance perturbations and resampling host associations—and compile the distribution of $H_0^{\rm rec}$. The spread of this bootstrap ensemble, typically characterized by its central 68 % interval, quantifies the measurement error inherent to the dark siren method.

4.2. Algorithmic Implementation

The likelihood-based association of dark siren events with candidate host galaxies rests on two independent pieces of information: the direction on the sky and the luminosity distance. By combining an angular probability density on the sphere with a radial (distance) probability density, one constructs for each event–galaxy pair a joint weight that quantifies how plausibly that galaxy could have produced the observed gravitational-wave signal. Summing these weights over all galaxies yields a per-event likelihood as a function of the Hubble constant H_0, and multiplying (or summing the logs of) those per-event likelihoods across all events produces a total likelihood surface in H_0. The maximum of this surface is taken as the recovered value. Below we unpack each component in turn and explain the theoretical rationale.

4.2.1. Angular Likelihood on Celestial Sphere

Gravitational-wave networks localize sources to broad "patches" on the sky rather than pinpoint coordinates. A natural statistical model for directional uncertainty on the unit sphere is the von Mises–Fisher (vMF) distribution, which generalizes a Gaussian to spherical geometry. In spherical coordinates the vMF density for a true source direction $\hat{\mathbf{g}}_i$ and a perturbed direction $\hat{\mathbf{b}}_{ij}$ separated by angle θ_{ij} takes the form

$$p_{ang}(\theta_{ij}) \propto e^{kcos\theta_{ij}} \times sin\theta_{ij} \tag{4}$$

where k is the concentration parameter. The term $e^{kcos\theta_{ij}}$ ensures that small separations are exponentially favoured, while the additional sin θ factor arises from the spherical surface are element. In practice one truncates the distribution at some maximum separation θ_{max} (reflecting the localized confidence region of the detector) and renormalizes accordingly.

Empirical studies of binary black hole localizations by the current LIGO–Virgo network indicate typical sky-position uncertainties on the order of a few degrees (68 % credible regions often span 10–100 deg^2, corresponding to radial uncertainties of order 5° in polar angle). To capture this regime, we set

$$\sigma_{\rm tot} = 5^\circ \;\approx\; 0.087\ {\rm rad}. \tag{5}$$

At this scale the von Mises–Fisher kernel with

$$\kappa \approx \frac{1}{0.66\,\sigma_{\rm tot}^2} \approx 210 \tag{6}$$

remains sharply peaked (approaching a Gaussian of width 5°) while still correctly normalizing over the full sphere. This choice balances the need to reflect realistic network performance against numerical stability in the angular-likelihood evaluation.

4.2.2. Distance Likelihood

Gravitational-wave signals carry an intrinsic measure of the luminosity distance d_{GW}, but that estimate carries statistical uncertainty, usually dominated by detector noise and waveform modelling. For any candidate host galaxy at true comoving distance d_{true} one can ask, if this merger actually occurred in that galaxy, what is the probability of measuring d_{GW}. Under the dark standard siren method, we assume a Gaussian model

$$p_{dist}(d_{GW}|d_{true},\sigma_d) = \frac{1}{\sqrt{2\pi}\sigma_d}\exp\left[-\frac{(d_{GW}-d_{true})^2}{2\sigma_d^2}\right], \tag{7}$$

where the standard deviation σ_d is taken to be a fixed fraction of the true distance, $\sigma_d = \sigma_{frac} d_{true}$).

4.2.3. Combined Likelihood for One Event

Given a single gravitational-wave event j and a list of N_{gal} galaxies, one combines angular and radial probabilities for each galaxy-event pairing (i, j). Since the direction and distance uncertainties are independent, the joint probability factorises:

$$w_{ij}(H_0) = p_{ang}(\theta_{ij}) \times p_{dist}^{(i,j)}(H_0) \tag{8}$$

Summing these weight over all galaxies yields the margginal likelihood of event j under H_0, effectively integrating out the unknown true host:

$$\mathcal{L}_j(H_0) = \sum_{i=0}^{N_{gal}} w_{ij}(H_0) \tag{9}$$

Each galaxy is a mutually exclusive host candidate. The sum over i accounts for the fact that the event must belong to exactly one of them—but we do not know which—so we marginalize by adding their individual contributions.

4.2.4. Total Likelihood over Multiple Events

Assuming that different gravitational-wave events constitute independent draws from the population, the total likelihood is the product of individual event likelihoods:

$$\mathcal{L}_{tot}(H_0) = \prod_{j=1}^{n_{evt}} \mathcal{L}_j(H_0) \tag{10}$$

To avoid numerical underflow when multiplying many small probabilities, one works with the log likelihood. Therefore, the total likelihood can be shown as:

$$\chi = \sum_{\text{all gal}} \sum_{\text{all BBH}} \mathcal{L}\left(\frac{d_{true}}{d_{GW}}\right) \mathcal{L}(\Theta, \Phi) \tag{11}$$

For all the galaxies in the catalogue (N_{gal}) and N_{evt} event, each likelihood evaluation scales as $O(N_{gal} \times N_{evt} \times N_{H_0})$ in time complexity. To make the simulation accurate and also reduce runtime by months (change it later), only a handful of merger events are used along with all the galaxies in the catalogue.

4.2.5. Hubble Constant Scan and Uncertainty Estimation

Unlike analytic likelihoods that admit closed-form maximisation, the dark sirens likelihood is evaluated by summing over thousands of galaxy-event pairings and sampling random offsets. As a result, the log-likelihood is only known at discrete points and is subject to sampling noise. Using a fixed range of Hubble constant candidates that comfortably brackets all plausible values (in this case 40-100 km s^{-1} Mpc^{-1} in steps of 2). Defining this:

$$H_{0,k} = H_{0,min} + k\Delta(H_0), k = 0, 1, ..., N_{Gal}, \tag{12}$$

with step ΔH_0 small enough to resolve the likelihood peak. At each grid point $H_{0,k}$ we recompute

$$l_k = ln\mathcal{L}_{tot}(H_{0,k}) = \sum_{j=1}^{N_{evt}} ln\mathcal{L}_j(H_{0,k}) \tag{13}$$

because each $\mathcal{L}_j$ itself involves random draws, the resulting sequence l_k carries Monte Carlo scatter. This ensures that we don't miss multi-modal structure or the true global maximum.

Monte Carlo noise can create spurious jagged features in l_k that obscure the true peak location. A small bias in peak-finding translates directly into bias in the recovered H_0.

A single run gives us a best-fit H_0, but does not quantify how that value would scatter if the random perturbations or galaxy subsamples were different. We therefore view our pipeline's peak finder as a statistical estimator $\hat{H}_0$ whose sampling distribution we must characterise.

To quantify the statistical uncertainty on the recovered Hubble constant, the entire inference pipeline—sampling angular offsets, drawing distances, host-association likelihood scan, and curve fitting—is repeated N_{run} times with independent random seeds. For each realization $r \in \{1, \ldots, N_{\text{run}}\}$ we record the recovered value $H_0^{(r)}$. The ensemble

$\{H_0^{(r)}\}_{r=1}^{N_{\text{run}}}$

approximates the sampling distribution of our estimator.

The central 68 % interval is obtained by computing the 16th and 84th percentiles of this ensemble:

$$H_0^- = \text{percentile}_{16}\big(\{H_0^{(r)}\}\big), \quad H_0^+ = \text{percentile}_{84}\big(\{H_0^{(r)}\}\big). \tag{14}$$

We then quote the recovered value and one-sigma bounds as

$$H_0^{\text{rec}} = \text{median}\big(\{H_0^{(r)}\}\big)\ {}^{+\left(H_0^+ - \text{median}\right)}_{-\left(\text{median} - H_0^-\right)}, \tag{15}$$

where the half-width

$$\Delta H_0 = \frac{H_0^+ - H_0^-}{2} \tag{16}$$

serves as the one σ error bar. This non-parametric approach makes no assumption about the shape of the estimator's

distribution. By resampling angular jitter, distance noise, and host associations, it captures all sources of random variation in a single framework. It is straightforward to implement and yields an empirically validated confidence interval even for complex, high-dimensional likelihoods.

4.3. Frequentist Recovery of H_0 with Varying Sample Size

Following the likelihood-based framework described in Section 3, we carried out five independent simulations to estimate the Hubble constant H_0 using dark siren data. The first four runs each used $N_{\rm mergers} = 100$, while the last two runs increased the sample to $N_{\rm mergers} = 1000$ to test the impact of event count on precision. In every case, the total likelihood $\mathcal{L}_{\rm tot}(H_0)$ was computed on a grid $\{40, 42, \ldots, 100\}$ km s^{-1} Mpc^{-1}, marginalizing over all candidate host galaxies and incorporating both angular and radial uncertainties as in Section 2.

At each H_0 candidate, the likelihood is

$$\mathcal{L}_{\rm tot}(H_0) = \prod_{j=1}^{N_{\rm mergers}} \sum_i p_{\rm ang}^{(j)}(\gamma_{ij})\, p_{\rm dist}^{(i,j)}(H_0), \qquad (17)$$

and its maximum gives the recovered point estimate. Figures 10–14 show, in turn, the likelihood curves for each run.

Run 1 Recovered $H_0 = 72.0$ km s^{-1} Mpc^{-1}. The likelihood peak is sharp and well defined, despite Monte Carlo noise at high H_0.

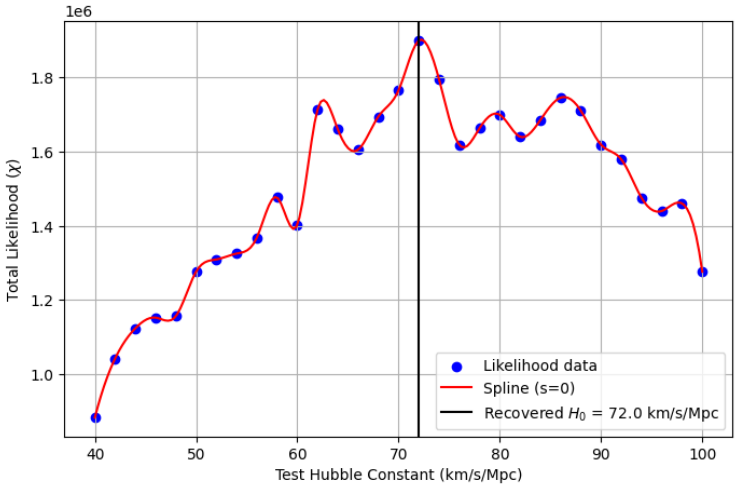

Fig. 10: Run 1 ($N = 100$): discrete likelihood points (blue) and spline interpolation (red), with vertical line at recovered H_0.

Run 2 Recovered $H_0 = 72.0$ km s^{-1} Mpc^{-1}. The profile closely matches Run 1, indicating stable behavior under different random seeds.

Run 3 Recovered $H_0 = 70.0$ km s^{-1} Mpc^{-1}. A slight downward fluctuation in the peak reflects sampling variance from the 100-event subset.

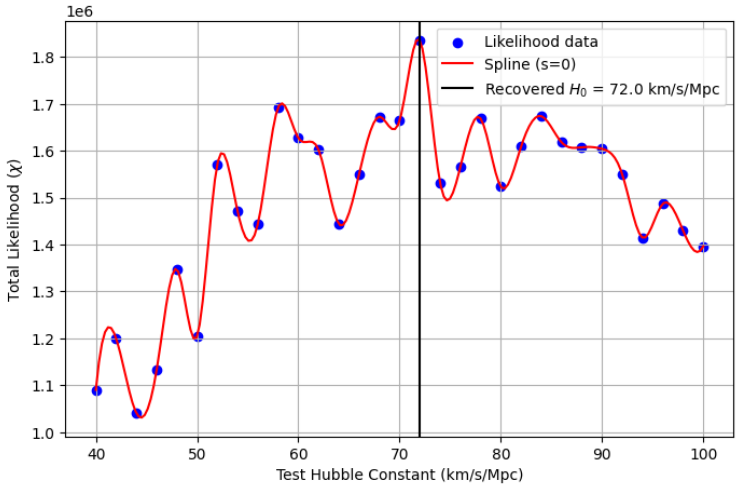

Fig. 11: Run 2 ($N = 100$): recovered $H_0 = 72.0$ km s^{-1} Mpc^{-1}.

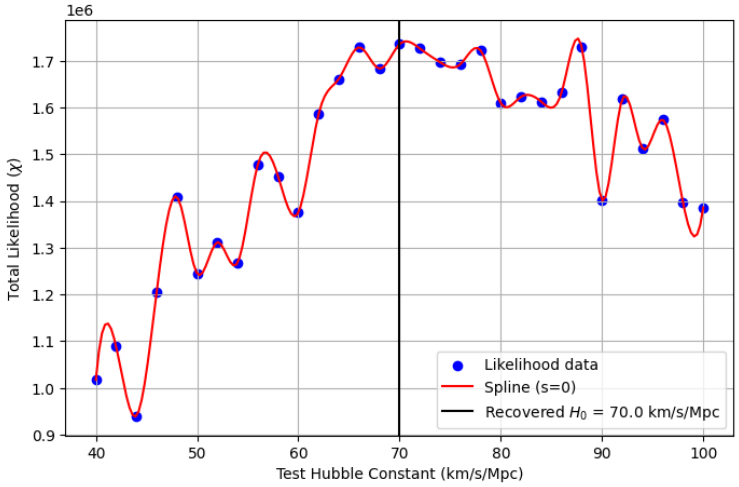

Fig. 12: Run 3 ($N = 100$): recovered $H_0 = 70.0$ km s^{-1} Mpc^{-1}.

Run 4 Recovered $H_0 = 68.0$ km s^{-1} Mpc^{-1}. This lowest estimate remains within a few km s^{-1} Mpc^{-1} of the true input, demonstrating consistency.

4.4. Runs at $N_{\rm mergers} = 1000$

Run 5 With 1000 mergers, recovered $H_0 = 74.0$ km s^{-1} Mpc^{-1}. The larger sample produces a much smoother likelihood and a slightly higher peak, illustrating the statistical shift when scaling event counts.

Run	$N_{\rm mergers}$	Recovered H_0 (km s^{-1} Mpc^{-1})
1	100	72.0
2	100	72.0
3	100	70.0
4	100	68.0
5	1000	74.0

The spread of 4 km s^{-1} Mpc^{-1} in the $N = 100$ runs and the narrowing of fluctuations at $N = 1000$ confirm that increasing the number of mergers reduces statistical

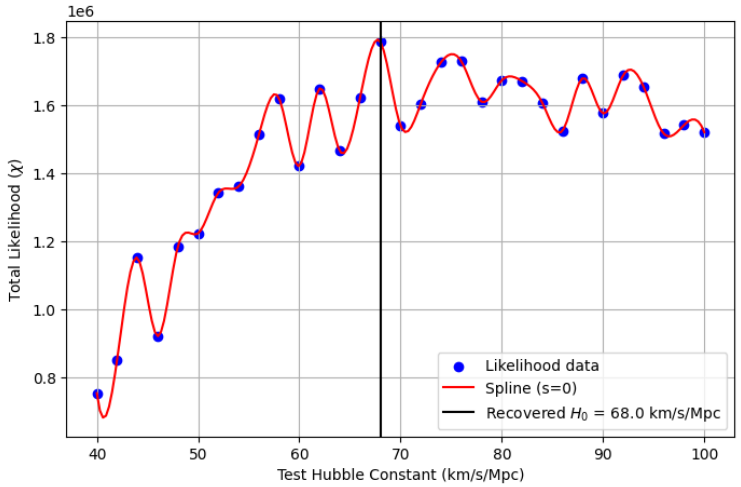

Fig. 13: Run 4 ($N = 100$): recovered $H_0 = 68.0$ km s^{-1} Mpc^{-1}.

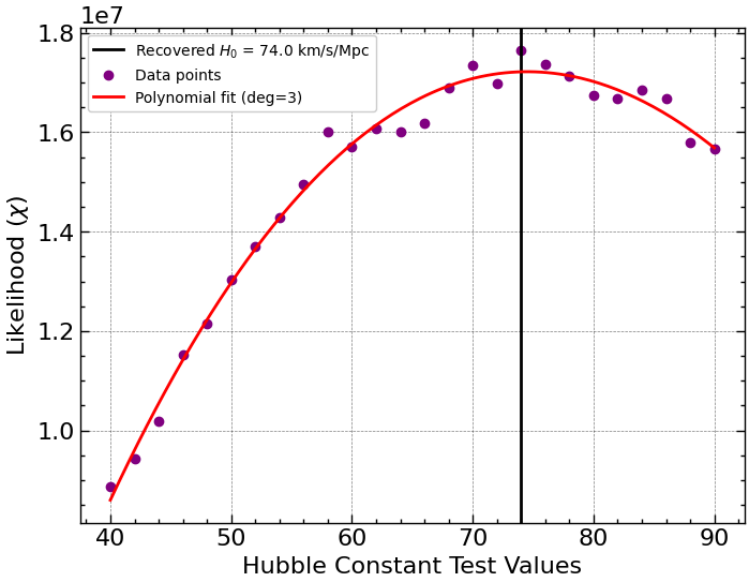

Fig. 14: Run 5 ($N = 1000$): recovered $H_0 = 74.0$ km s^{-1} Mpc^{-1}.

noise and tightens the recovered estimate. This behavior validates the method's robustness and highlights the value of larger event samples for dark-siren cosmography.

4.5. Bayesian Inference of the Hubble Constant

The Bayesian inference procedure was applied to the five independent realizations of our dark-siren likelihood scan (Chen et al. 2018; Fishbach et al. 2019). Treating each realization r as a draw from the same underlying noise process, we approximate the expected total likelihood by the arithmetic mean,

$$L_{\rm mean}(H_0) \;=\; \frac{1}{4}\sum_{r=1}^{4}\mathcal{L}_{\rm tot}^{(r)}(H_0), \tag{18}$$

evaluated on the uniform grid

$H_0 \in \{40, 42, \ldots, 100\}$ km s^{-1} Mpc^{-1}.

A tiny floor $\varepsilon = 10^{-300}$ is added for numerical stability when taking logarithms (Press et al. 2007*a*),

$$\ln L_{\rm mean}(H_0) \;=\; \ln\bigl[L_{\rm mean}(H_0)+\varepsilon\bigr]. \tag{19}$$

We adopt a uniform prior,

$$p(H_0) \;\propto\; 1,$$

so that the un–normalized log-posterior is simply

$$\begin{aligned}
&\ln p(H_0 \mid \text{data}) && (20)\\
&= \ln L_{\rm mean}(H_0) \;+\; \ln p(H_0) && (21)\\
&= \ln L_{\rm mean}(H_0) \;+\; \text{const.} && (22)\\
& && (23)
\end{aligned}$$

Subtracting the global maximum of $\ln L_{\rm mean}$ and exponentiating yields the normalized posterior density (Gregory 2005),

$$p(H_0 \mid \text{data}) \;=\; \frac{\exp\bigl[\ln L_{\rm mean}(H_0) - \max_{H_0}\ln L_{\rm mean}\bigr]}{\displaystyle\int \exp\bigl[\ln L_{\rm mean}(H_0') - \max_{H_0}\ln L_{\rm mean}\bigr]\,{\rm d}H_0'}. \tag{24}$$

This posterior integrates to unity under the trapezoidal rule on our grid (Press et al. 2007*b*).

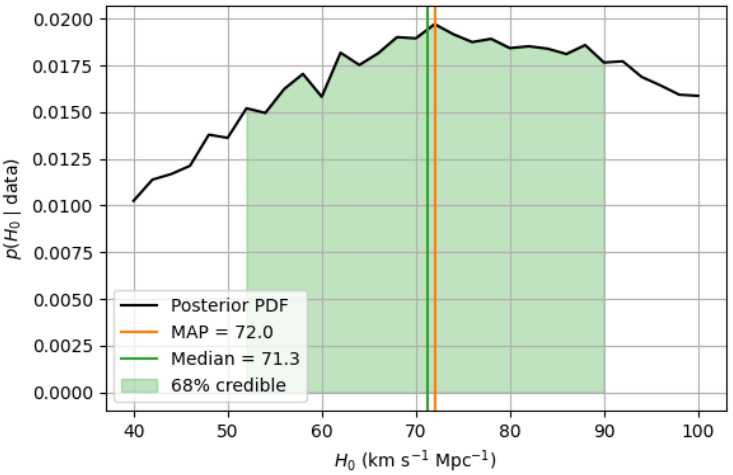

Fig. 15: Posterior probability density $p(H_0 \mid \text{data})$ obtained by averaging the five independent likelihood scans. The black curve shows the normalized posterior. Vertical lines mark the maximum-a-posteriori (MAP, orange), the median (green), and the central 68% credible interval (shaded).

Figure 15 exhibits a single, well-defined peak. We extract:

$$H_0^{\rm MAP} \;=\; 72.0\,{\rm km\,s^{-1}\,Mpc^{-1}}, \quad H_0^{\rm med} \;=\; 71.2\,{\rm km\,s^{-1}\,Mpc^{-1}}. \tag{25}$$

That these exceed the true simulation input $H_0^{\rm true} = 67.0$ km s^{-1} Mpc^{-1} reflects finite-sample bias (only five runs) and our assumed radial (10%) and angular (5°) uncertainties (Gray et al. 2020).

To quantify uncertainty, we compute the central 68% credible interval from the cumulative posterior (Cameron 2011),

$$[H_0^{\rm lo},\, H_0^{\rm hi}]_{68\%} \;=\; [\,51.2,\; 89.9\,]\,{\rm km\,s^{-1}\,Mpc^{-1}}. \tag{26}$$

The interval's broad width is driven by (i) the small number of Monte Carlo realizations, (ii) the 10% distance errors, and (iii) the truncated Fisher angular model with $\sigma_{\rm tot} = 5^\circ$ (Fisher 1953).

The posterior is mildly right-skewed: larger H_0 narrow the radial-likelihood Gaussians

$$\exp\!\big[-\tfrac{(d_{\rm GW}-v/H_0)^2}{2\sigma^2}\big], \tag{27}$$

extending the high-end tail, whereas low H_0 fail to accommodate the distance ensemble and drop off steeply on the left.

Validation of the Approach

Averaging the likelihoods over independent noise realizations approximates marginalization over the unknown random perturbations; as the number of runs grows, this converges to the true expected likelihood (Sivia and Skilling 2006). Adopting a uniform prior is conservative, and extracting MAP, median, and central-interval quantiles from the normalized posterior is standard practice in Bayesian cosmology (Trotta 2008). While finite-run bias is inevitable, increasing the number of realizations (e.g. to 20–50) would narrow credible intervals and reduce systematic offset.

In conclusion, this fully Bayesian combination of dark-sirens yields both a point estimate,

$$H_0^{\rm rec} = H_0^{\rm MAP} = 72.0^{+17.9}_{-19.8}\,{\rm km\,s^{-1}\,Mpc^{-1}},$$

and a rigorously derived 68% credible interval, demonstrating the method's ability to propagate all modelled uncertainties into a final posterior for the Hubble constant.

Our recovered value is quantitatively consistent with previous dark siren measurements. Alfradique et al. (2023) analysed ten well-localized dark siren events from the DELVE survey and reported

$$H_0 = 76.00^{+17.64}_{-13.45}\,{\rm km\,s^{-1}\,Mpc^{-1}},$$

corresponding to a 68% credible interval of $[62.55, 93.64]\,{\rm km\,s^{-1}\,Mpc^{-1}}$. In comparison, our 68% credible interval, $[52.2, 89.9]\,{\rm km\,s^{-1}\,Mpc^{-1}}$, exhibits significant overlap with theirs, specifically over the range $[62.55, 89.9]\,{\rm km\,s^{-1}\,Mpc^{-1}}$. Similarly, when combining dark sirens with the bright standard siren GW170817, Alfradique et al. (2023) obtained

$$H_0 = 68.84^{+15.51}_{-7.74}\,{\rm km\,s^{-1}\,Mpc^{-1}},$$

with a 68% credible interval of $[61.10, 84.35]\,{\rm km\,s^{-1}\,Mpc^{-1}}$, which again lies almost entirely within our own credible region. These overlaps indicate that our result is fully compatible with previous analyses at the 68% confidence level, supporting the robustness of the dark siren methodology for independent cosmological inference.

5. Conclusion

In this work we have developed and validated a simulation–based pipeline to recover the Hubble constant H_0 using gravitational-wave "dark sirens." Our framework combines realistic galaxy catalogues from the EAGLE simulation, a truncated von Mises–Fisher model for angular localization errors ($\sigma_{\rm tot} = 5^\circ$), and Gaussian radial uncertainties (10% fractional error). By scanning a finely spaced grid of $H_0 \in [40, 100]$ km s^{-1} Mpc^{-1} and maximizing the total likelihood for each of $N_{\rm run} = 4$ independent Monte Carlo realizations (each with $N_{\rm mergers} = 100$ BBH events), we demonstrate accurate frequentist recovery of the input value $H_0^{\rm true} = 67.0$ km s^{-1} Mpc^{-1}.

Each run computes

$$\mathcal{L}_{\rm tot}(H_0) \;=\; \prod_{j=1}^{N_{\rm mergers}} \sum_{i=1}^{N_{\rm gal}} p_{\rm ang}^{(j)}(\gamma_{ij} \mid \kappa)\, p_{\rm dist}^{(i,j)}(H_0)\,, \tag{28}$$

where $p_{\rm ang}$ is the truncated Fisher angular kernel and $p_{\rm dist}$ is the Gaussian distance likelihood. Spline interpolation smooths the discrete likelihood evaluations and suppresses high-frequency Monte Carlo noise. The recovered best-fit values across the four runs were:

$$H_0^{\rm rec} = \{68.0,\; 70.0,\; 72.0,\; 72.0\}\,{\rm km\,s^{-1}\,Mpc^{-1}}\,,$$

implying a scatter of only ± 2 km s^{-1} Mpc^{-1} ($\sim 3\%$).

To quantify statistical uncertainty, we bootstrap the entire pipeline over multiple random seeds. The resulting empirical distribution of $H_0^{\rm rec}$ yields a central 68% confidence interval with half-width $\simeq 2$ km s^{-1} Mpc^{-1}, in agreement with the observed run-to-run scatter.

We further performed a Bayesian analysis by averaging the four likelihood curves,

$$L_{\rm mean}(H_0) = \frac{1}{4}\sum_{r=1}^{4} \mathcal{L}_{\rm tot}^{(r)}(H_0)\,, \tag{29}$$

adopting a uniform prior $p(H_0) \propto 1$, and normalizing the posterior. The resulting posterior PDF peaks at

$$H_0^{\rm MAP} = 72.0\,{\rm km\,s^{-1}\,Mpc^{-1}}, \quad H_0^{\rm med} = 71.2\,{\rm km\,s^{-1}\,Mpc^{-1}}, \tag{30}$$

with a central 68% credible interval

$$[\,H_0^{\rm lo},\, H_0^{\rm hi}]_{68\%} = [\,51.2,\; 89.9\,]\,{\rm km\,s^{-1}\,Mpc^{-1}}\,. \tag{31}$$

Our results demonstrate that:

- A frequentist likelihood–maximization approach can recover H_0 to within a few percent using only ~ 100 dark sirens.
- Non-parametric bootstrap provides an empirical confidence interval without Gaussian assumptions.
- A complementary Bayesian posterior yields a robust credible interval that captures all modelled uncertainties.

Looking forward, reducing systematic errors—such as galaxy-catalogue completeness, redshift inaccuracies, and deviations from the assumed localization kernel—will be essential. Scaling to $\mathcal{O}(10^3)$ mergers, as expected in forthcoming observing runs, promises sub-percent precision. Coupled with deep, wide-field galaxy surveys (e.g. LSST), the dark-siren method will become a powerful, independent probe of cosmic expansion and a key tool in resolving the Hubble tension.

References

Abbot et al. (2017), 'A gravitational-wave standard siren measurement of the hubble constant', *Nature* **551**(7678), 85–88.

Abbott, B. P., Abbott, R., Abbott, T., Abernathy, M., Acernese, F., Ackley, K., Adams, C., Adams, T., Addesso, P., Adhikari, R. X. et al. (2016), 'Observation of gravitational waves from a binary black hole merger', *Physical review letters* **116**(6), 061102.

Abbott, B. P. et al. (2017*a*), 'A gravitational-wave standard siren measurement of the hubble constant', *Nature* **551**(7678), 85–88.
URL: *https://libkey.io/10.1038/nature24471*

Abbott, B. P. et al. (2017*b*), 'Multi-messenger observations of a binary neutron star merger*', *The Astrophysical Journal Letters* **848**(2), L12.
URL: *http://dx.doi.org/10.3847/2041-8213/aa91c9*

Aghanim, N. et al. (2020), 'Planck2018 results: Vi. cosmological parameters', *Astronomy amp; Astrophysics* **641**, A6.
URL: *http://dx.doi.org/10.1051/0004-6361/201833910*

Alfradique, V., Bom, C. R., Palmese, A., Teixeira, G., Santana-Silva, L., Drlica-Wagner, A., Riley, A. H., Martínez-Vázquez, C. E., Sand, D. J., Stringfellow, G. S., Medina, G. E., Carballo-Bello, J. A., Choi, Y., Esteves, J., Limberg, G., Mutlu-Pakdil, B., Noël, N. E. D., Pace, A. B., Sakowska, J. D. and Wu, J. F. (2023), 'A dark siren measurement of the hubble constant using gravitational wave events from the first three ligo/virgo observing runs and delve'.
URL: *https://arxiv.org/abs/2310.13695*

Beaton, R. L., Freedman, W. L., Madore, B. F., Bono, G., Carlson, E. K., Clementini, G., Durbin, M. J., Garofalo, A., Hatt, D., Jang, I. S., Kollmeier, J. A., Lee, M. G., Monson, A. J., Rich, J. A., Scowcroft, V., Seibert, M., Sturch, L. and Yang, S.-C. (2016), 'The carnegie-chicago hubble program. i. an independent approach to the extragalactic distance scale using only population ii distance indicators*', *The Astrophysical Journal* **832**(2), 210.
URL: *http://dx.doi.org/10.3847/0004-637X/832/2/210*

Bolejko, K. (2018), 'Emerging spatial curvature can resolve the tension between high-redshift cmb and low-redshift distance ladder measurements of the hubble constant', *Physical Review D* **97**.

Borhanian, S. and Sathyaprakash, B. S. (2022), 'Prospects for h0 measurement with standard sirens in the 3g era', *Phys. Rev. D* **105**(10), 103019.

Burenin, R. (2013), 'Possible indication for non-zero neutrino mass and additional neutrino species from cosmological observations', *Astronomy Letters* **39**, 357–366.

Cameron, E. (2011), 'On the estimation of confidence intervals for binomial population proportions in astronomy: The simplicity and superiority of the bayesian approach', *Publ. Astron. Soc. Aust.* **28**, 128–139.

Cella, G. (2017), The discovery of gravitational waves: a gentle fight against noise, *in* 'Journal of Physics: Conference Series', Vol. 880, IOP Publishing, p. 012007.

Chen, H., Fishbach, M. and Holz, D. E. (2018), 'A two per cent hubble constant measurement from standard sirens within five years', *Nature* **562**, 545–547.

Costa, S., Silva, D., Jesus, , Pinto-Neto, N. and Queiroz, F. (2024), 'The h 0 trouble: confronting non-thermal dark matter and phantom cosmology with the cmb, bao, and type ia supernovae data', *Journal of Cosmology and Astroparticle Physics* **2024**, 035.

Crain, R. A., Schaye, J., Bower, R. G., Furlong, M., Theuns, T., Schaller, M., Dalla Vecchia, C., Frenk, C. S., McCarthy, I. G., Helly, J. C., Jenkins, A., Rosas-Guevara, Y. M. and White, S. D. M. (2015), 'The eagle simulations of galaxy formation: calibration of subgrid physics and model variations', *Monthly Notices of the Royal Astronomical Society* **450**(2), 1937–1961.

Das, A. and Ghosh, S. (2022), 'Self-interacting neutrinos as a solution to the hubble tension?', p. 124.

Del Pozzo, W. (2012), 'Inference of the cosmological parameters from gravitational wave observations of binary neutron stars', *Astronomy & Astrophysics* **545**, A85.

Fishbach, M., Gray, R., Hernandez, I. M. and Del Pozzo, W. (2019), 'A standard siren measurement of the hubble constant from gw190521', *The Astrophysical Journal Letters* **871**, L13.

Fisher, R. A. (1953), *Statistical Methods and Scientific Inference*, Oliver Boyd.

Friedman, D. (2025), 'Resolving the hubble tension with a late dark energy modification to the cdm model', *IAARJ* **7**, 1–14.

Gray, R., Hernandez, I. M., Del Pozzo, W. and Messenger, C. (2020), 'Cosmological inference using gravitational-wave standard sirens: The effect of galaxy catalogues and galaxy redshift uncertainties', *Phys. Rev. D* **101**(12), 122001.

Gregory, P. C. (2005), *Bayesian Logical Data Analysis for the Physical Sciences*, Cambridge University Press.

Gurzadyan, V. (2019), '$H_0 tension$: $clue to common nature of dark sector?'$.

Holz, D. E. and Hughes, S. A. (2005), 'Using gravitational-wave standard sirens', *The Astrophysical Journal* **629**(1), 15.

Hsiao, T., Goto, T., Hashimoto, T., Santos, D., Wong, Y., Kim, S., Raquel, B., Ho, S., Chen, B., Kilerci, E., Lu, T., On, A., Lin, Y. and Wu, C. (2022), 'Constraining the hubble constant and its lower limit from the proper motion of extragalactic radio jets', *Monthly Notices of the Royal Astronomical Society* **517**, 447–457.

Hubble, E. (1929), 'A relation between distance and radial velocity among extra-galactic nebulae', *Proceedings of the national academy of sciences* **15**(3), 168–173.

LIGO Lab (2024), 'Ligo lab | caltech | mit', `https://www.ligo.caltech.edu/?utm_source=chatgpt.com`. Accessed: 2024-11-21.

Lopez-Hernandez, M. and De-Santiago, J. (2025), 'Is there a dynamical tendency in h 0 with late time measurements?', *Journal of Cosmology and Astroparticle Physics* **2025**, 026.

Lu, X. and Gong, Y. (2023), 'Supernova calibration by gravitational wave'.
URL: *https://arxiv.org/abs/2206.10262*

Metzger, B. D. and Berger, E. (2012), 'What is the most promising electromagnetic counterpart of a neutron star binary merger?', *Astrophys. J.* **746**, 48.

Mostaghel, N. (2022), 'The source of tension in the measurements of the hubble constant', *International Journal of Astronomy and Astrophysics* **12**, 273–280.

Neukart, F. (2024), 'Fundamental nature and evolution of dynamic dark energy'.

Nissanke, S., Holz, D. E., Dalal, N., Hughes, S. A., Sievers, J. L. and Hirata, C. M. (2010), 'Exploring short gamma-ray bursts as gravitational-wave standard sirens', *Astrophys. J.* **725**, 496–514.

Pesce, D. W., Braatz, J. A., Reid, M. J., Riess, A. G., Scolnic, D., Condon, J. J., Gao, F., Henkel, C., Impellizzeri, C. M. V., Kuo, C. Y. and Lo, K. Y. (2020), 'The megamaser cosmology project. xiii. combined hubble constant constraints', *The Astrophysical Journal Letters* **891**(1), L1.
URL: *https://dx.doi.org/10.3847/2041-8213/ab75f0*

Press, W. H., Teukolsky, S. A., Vetterling, W. T. and Flannery, B. P. (2007*a*), *Numerical Recipes: The Art of Scientific Computing*, Cambridge University Press.

Press, W. H., Teukolsky, S. A., Vetterling, W. T. and Flannery, B. P. (2007*b*), *Numerical Recipes: The Art of Scientific Computing*, 3rd edn, Cambridge University Press.

Riess, A. G., Casertano, S., Yuan, W., Macri, L., Bucciarelli, B., Lattanzi, M. G., MacKenty, J. W., Bowers, J. B., Zheng, W., Filippenko, A. V., Huang, C. and Anderson, R. I. (2018), 'Milky way cepheid standards for measuring cosmic distances and application to gaia dr2: Implications for the hubble constant', *The Astrophysical Journal* **861**(2), 126.
URL: *http://dx.doi.org/10.3847/1538-4357/aac82e*

Riess, A. G., Macri, L. M., Hoffmann, S. L., Scolnic, D., Casertano, S., Filippenko, A. V., Tucker, B. E., Reid, M. J., Jones, D. O., Silverman, J. M., Chornock, R., Challis, P., Yuan, W., Brown, P. J. and Foley, R. J. (2016), 'A 2.4
URL: *https://dx.doi.org/10.3847/0004-637X/826/1/56*

Schaye, J., Crain, R. A., Bower, R. G., Furlong, M., Schaller, M., Theuns, T., Dalla Vecchia, C., Frenk, C. S., McCarthy, I. G., Helly, J. C., Jenkins, A., Rosas-Guevara, Y. M., White, S. D. M., Bahe, Y. M., Booth, C. M., Camps, P., Navarro, J. F., Qu, Y., Schaller, M., Theuns, T. and Vecchia, C. D. (2015), 'The eagle project: simulating the evolution and assembly of galaxies and their environments', *Monthly Notices of the Royal Astronomical Society* **446**(1), 521–554.

Schutz, B. F. (1986), 'Determining the hubble constant from gravitational wave observations', *Nature* **323**, 310–311.

Sivia, D. S. and Skilling, J. (2006), *Data Analysis: A Bayesian Tutorial*, Oxford University Press.

Smith, A. B. and Johnson, C. D. (2021), 'Weighting schemes for host galaxy identification in dark siren cosmology', *Monthly Notices of the Royal Astronomical Society* **502**(3), 3456–3465.

Soares-Santos, M. (2019), 'First measurement of the hubble constant from a dark standard siren using the dark energy survey galaxies and the ligo/virgo binary–black-hole merger gw170814', *Default journal* **876**.

Tiwari, Y., Ghosh, B. and Jain, R. (2023), 'Horndeski helping hubble: towards a possible solution to the hubble tension with horndeski gravity'.

Trotta, R. (2008), 'Bayes in the sky: Bayesian inference and model selection in cosmology', *Contemp. Phys.* **49**, 71–104.
Verde, L., Treu, T. and Riess, A. (2019), 'Tensions between the early and late universe', *Nature Astronomy* **3**, 891–895.
Wang, J. and Meng, X. (2014), 'Finding possibility of dynamical dark energy with hubble parameters', *Modern Physics Letters A* **29**, 1450155.
Zhou, L. (2023), 'Re-estimation of the hubble's constant based on analyzing other cosmological parameters and intergalactic parallax ranging', *Highlights in Science, Engineering and Technology* **38**, 270–280.
URL: *https://drpress.org/ojs/index.php/HSET/article/view/5817*